New Probes of the F_1-ATPase Catalytic Transition State Reveal That Two of the Three Catalytic Sites Can Assume a Transition State Conformation Simultaneously†

Sashi Nadanaciva, Joachim Weber, and Alan E. Senior*

Department of Biochemistry and Biophysics, University of Rochester Medical Center, Box 712, Rochester, New York 14642

Received April 25, 2000; Revised Manuscript Received June 6, 2000

ABSTRACT: MgADP in combination with fluoroscandium (ScFx) is shown to form a potently inhibitory, tightly bound, noncovalent complex at the catalytic sites of F_1-ATPase. The F_1·MgADP·ScFx complex mimics a catalytic transition state. Notably, ScFx caused large enhancement of MgADP binding affinity at both catalytic sites 1 and 2, with little effect at site 3. These results indicate that sites 1 and 2 may form a transition state conformation. A new direct optical probe of F_1-ATPase catalytic transition state conformation is also reported, namely, substantial enhancement of fluorescence emission of residue β-Trp-148 observed upon binding of MgADP·ScFx or MgIDP·ScFx. Using this fluorescence signal, titrations were performed with MgIDP·ScFx which demonstrated that catalytic sites 1 and 2 can both form a transition state conformation but site 3 cannot. Supporting data were obtained using MgIDP−fluoroaluminate. Current models of the MgATP hydrolysis mechanism uniformly make the assumption that only one catalytic site hydrolyzes MgATP at any one time. The fluorometal analogues demonstrate that two sites have the capability to form the transition state simultaneously.

Studies of the catalytic mechanism of ATP- and GTP-hydrolyzing enzymes have profited from utilization of beryllium fluoride (BeFx),[1] aluminum fluoride (AlFx), and orthovanadate (Vi). In association with Mg−nucleoside diphosphate, these compounds form tightly bound, potently inhibitory complexes in the catalytic sites of the enzyme, which mimic intermediates of the nucleotide hydrolysis pathway. The BeFx−nucleoside diphosphate complex mimics the bound nucleoside triphosphate ground state (*3*−*5*), whereas AlFx− and Vi−nucleoside diphosphate complexes mimic the catalytic transition state (*6*−*12*). Not only have these analogues facilitated X-ray structural analyses and understanding of catalytic mechanism, they have also been of importance in understanding energy coupling between ATP/GTP hydrolysis and functions as diverse as large protein domain movement in myosin (*13*), signaling in G-proteins (*14*), and electron transfer in nitrogenase (*14*).

F_1F_o-ATP synthase is the enzyme responsible for ATP synthesis in oxidative phosphorylation and photophosphorylation in mitochondria, chloroplasts, or bacteria and also for ATP-driven proton pumping across bacterial membranes when metabolic conditions require (*15*, *16*). In this large multisubunit enzyme, ATP hydrolysis in the F_1 sector has been shown to drive rotation of certain subunits (*17*−*19*), and the rotational energy is transduced within the F_o sector into proton pumping across the membrane (*20*−*22*). The catalytic mechanism of ATP hydrolysis and its transduction into rotational movement of subunits is not yet understood. From experience with other enzymes, as discussed above, it seems likely that use of fluorometal−nucleoside diphosphate complexes as analogues of catalytic intermediates will shed light not only on the catalytic mechanism but also on the coupling of ATP hydrolysis to subunit rotation.

Published data establish that MgADP·BeFx, MgADP·AlFx, and MgADP·Vi potently inhibit F_1-ATPase (*23*−*27*) and show that the latter two complexes mimic the catalytic transition state. We recently analyzed the transition state of *Escherichia coli* F_1 by monitoring binding of MgADP·AlFx, using the genetically engineered residue β-Trp-331[2] as an intrinsic fluorescence probe of nucleotide binding (*28*). We found that AlFx profoundly enhanced MgADP binding affinity at catalytic site 1, caused moderate enhancement of affinity at site 2, and had no influence at site 3 (*29*). In contrast, the mutant enzymes βK155Q/βY331W, βE181Q/βY331W, βR182Q/βY331W, αR376Q/βY331W, and αR376C/βY331W, each of which involves modification of a critical catalytic residue side chain, did not show enhanced affinity for MgADP in the presence of AlFx (*29*−*31*) at any of the three sites. On the basis of these results, we proposed a model in which residues β-Lys-155, β-Arg-182, α-Arg-376, and β-Glu-181 stabilize the catalytic transition state during MgATP hydrolysis (*31*). X-ray structural analysis of bovine heart mitochondrial F_1 with bound MgADP·AlF_3 concurs with this model (*32*). However, while available data clearly show formation of a transition state at catalytic site 1 (the site of highest affinity for substrate), the question as to whether a partial or true catalytic transition state forms at catalytic site 2 is not yet settled.

† Supported by NIH Grant GM25349 to A.E.S.

* To whom correspondence should be addressed: 716-275-2777 (phone); 716-271-2683 (fax); alan_senior@urmc.rochester.edu (e-mail).

[1] Abbreviations: BeFx, beryllium fluoride (fluoroberyllate) (the exact composition of this complex in F_1-ATPase is not yet known; see refs *1* and *2*); AlFx, aluminum fluoride (fluoroaluminate) (in different enzymes this has been seen by X-ray crystallography to involve either AlF_3 or AlF_4^- (*3*−*12*); Vi, orthovanadate; ScFx, scandium fluoride (fluoroscandium).

[2] *E. coli* residue numbers are used throughout.

10.1021/bi000941o CCC: $19.00
Published on Web 07/08/2000

Recently, it was demonstrated that scandium fluoride (ScFx) with MgADP forms a tight and potently inhibitory complex that mimics the transition state of ATP hydrolysis in myosin (*33*−*35*). The length of the Sc to oxygen bond is known from small molecule crystallography to be 2.07−2.18 Å (*36*, *37*), which is similar to the Al to oxygen bond (2.00 Å) in the myosin·MgADP·AlF_4^- complex (*3*) and also to the V to oxygen bond (2.09 Å) in the myosin·MgADP·Vi complex (*6*). In contrast, the Be to oxygen distance (1.57 Å) of the myosin·MgADP·BeFx complex (*3*) is similar to that of the Pγ to ADP−O bridge oxygen in ATP, and this complex is thought to mimic the bound MgATP ground state. Notably, the three transition state mimics, MgADP·Vi, MgADP·AlF_4^-, and MgADP·ScFx, each produced different degrees of domain movement within the myosin molecule, and the degree of movement was correlated with the metal to oxygen bond length (*35*), demonstrating the value of using multiple probes.

To date, there have been no investigations of effects of ScFx on F_1-ATPase, and the first goal of this paper was to establish whether MgADP·ScFx could provide an alternative and useful probe of the catalytic transition state in *E. coli* F_1-ATPase. The data confirm that it does. A second goal was to obtain a direct optical probe of the transition state. Fluorescence of β-Trp-148 in the βF148W mutant enzyme was shown previously to respond differentially to nucleoside triphosphate vs nucleoside diphosphate bound at catalytic sites (*38*). Here, using ScFx, we demonstrate that β-Trp-148 fluorescence also responds uniquely to the catalytic transition state. By combined use of ScFx and β-Trp-148 probes, we then test whether both catalytic sites 1 and 2 are able to assume the transition state.

EXPERIMENTAL PROCEDURES

Strains of E. coli Used. Wild-type *E. coli* F_1 and mutant F_1 enzymes βY331W, βT156A/βY331W, βK155Q/βY331W, αR376Q/βY331W, and βF148W were prepared from strains SWM1 (*39*), SWM4 (*28*), STH1 (*40*), SWM31 (*41*), SN3 (*31*), and RLL3 (*42*).

Preparation of Enzymes. F_1 was purified as described (*43*). Prior to use, all enzymes were passed through two 1 mL centrifuge columns of Sephadex G-50 in 50 mM Tris−SO_4, pH 8.0, to deplete the catalytic sites of bound nucleotide (*44*). Nucleotide-depleted F_1 (depleted of both catalytic- and noncatalytic-site-bound nucleotide) was prepared according to Senior et al. (*45*). Specific ATPase activities (20 °C, pH 8.5) were as follows: wild-type, 22 units/mg; βY331W, 8 units/mg; βF148W, 20 units/mg. βT156A/βY331W, βK155Q/βY331W, and αR376Q/βY331W were all essentially zero.

Inhibition of F_1-ATPase by MgADP·ScFx. F_1 was preincubated at room temperature in 50 mM Tris−SO_4, pH 8.0, with additions of $MgSO_4$, $ScCl_3$, NaF, and NaADP as described in Results. Aliquots were removed, and ATPase activity was measured in 50 mM Tris−SO_4, pH 8.5, 10 mM NaATP, and 4 mM $MgCl_2$, in a total volume of 1 mL for 3−5 min at room temperature, after which the reaction was stopped with 1 mL of 10% (w/v) sodium dodecyl sulfate. Phosphate release was measured as in ref *46*. All reactions were linear with time and protein concentration.

Fluorescence Measurements. Fluorescence measurements were made in a SPEX Fluorolog 2 or Aminco-Bowman 2 spectrofluorometer. The excitation wavelength was 295 nm. The fluorescence emission for βY331W-containing mutant enzymes (β-Trp-331 fluorescence) was measured at 360 nm, while for βF148W mutant F_1, fluorescence emission spectra between 310 and 380 nm were recorded. The final F_1 concentration in the cuvette was 30−150 nM. All fluorescence measurements were made at room temperature in 50 mM Tris−SO_4, pH 8.0. MgADP titrations were done in buffer containing 2.5 mM $MgSO_4$, and then NaADP was added in increments. MgADP titrations in the presence of ScFx were carried out in buffer containing 2.5 mM $MgSO_4$, 0.3 mM $ScCl_3$, and 10 mM NaF, and then NaADP was added. Enzyme was incubated for 60 min before fluorescence measurements were made. Inner filter and volume effects were corrected by performing parallel titrations with wild-type F_1, and background signals due to buffer were subtracted. Nucleotide binding parameters were analyzed by fitting theoretical curves to the measured data points, assuming theoretical models with one, two, or three types of binding sites as described in ref *41*. MgADP concentrations were calculated using the stability constant of 78 μM (*29*).

Materials. $ScCl_3$ (99.9% pure) was from Aldrich (catalog number 30785-8).

Table 1: Inhibition of *E. coli* F_1 by MgADP−Fluoroscandium[a]

additions	ATPase activity (%)
none	100
2.5 mM $MgSO_4$, 1 mM NaADP, 0.3 mM $ScCl_3$	91
2.5 mM $MgSO_4$, 1 mM NaADP, 10 mM NaF	88
2.5 mM $MgSO_4$, 1 mM NaADP, 0.3 mM $ScCl_3$, 10 mM NaF	5
2.5 mM $MgSO_4$, 1 mM NaGDP, 0.3 mM $ScCl_3$, 10 mM NaF	8
2.5 mM $MgSO_4$, 1 mM NaIDP, 0.3 mM $ScCl_3$, 10 mM NaF	6
no $MgSO_4$, 1 mM NaADP, 0.3 mM $ScCl_3$, 10 mM NaF	91
2.5 mM $MgSO_4$, 0.3 mM $ScCl_3$, 10 mM NaF	45
2.5 mM $MgSO_4$, 0.3 mM $ScCl_3$, 10 mM NaF	70[b]
2.5 mM $MgSO_4$, 0.3 mM $ScCl_3$, 10 mM NaF	77[c]

[a] Wild-type *E. coli* F_1 was passed through two 1 mL centrifuge columns of Sephadex G-50 in 50 mM Tris−SO_4, pH 8.0, and preincubated at room temperature for 60 min in 50 mM Tris−SO_4, pH 8.0, containing the additions indicated. 100 μL aliquots (4−8 μg) were removed and assayed for ATPase activity in 50 mM Tris−SO_4, pH 8.5, 10 mM NaATP, and 4 mM $MgCl_2$ in a total volume of 1 mL as described in Experimental Procedures. Phosphate release was measured as described in ref *47*. [b] Nucleotide-depleted F_1 prepared as in ref *46*. [c] Treated to remove nucleotide as follows. F_1 was passed through one centrifuge column in 50 mM Tris−SO_4 and 0.5 mM EDTA, pH 8.0, incubated at 20 °C for 1 h with additional 4 mM EDTA, and then passed sequentially through two centrifuge columns in 50 mM Tris−SO_4 and 0.5 mM EDTA, pH 8.0.

RESULTS

ATPase Activity of E. coli F_1 Is Inhibited by MgADP plus Scandium Fluoride. The results for wild-type enzyme are displayed in Table 1. MgADP plus either $ScCl_3$ or NaF produced only ~10% inhibition (lines 2 and 3), which is due to competitive inhibition by MgADP carried over from the preincubation into the ATPase assay, plus minor inhibition of a few percent seen with $ScCl_3$ and NaF alone. Addition of MgADP with both $ScCl_3$ and NaF together produced strong (95%) inhibition (line 4), showing that ScFx (ScFx) was the inhibitory agent. MgGDP and MgIDP were

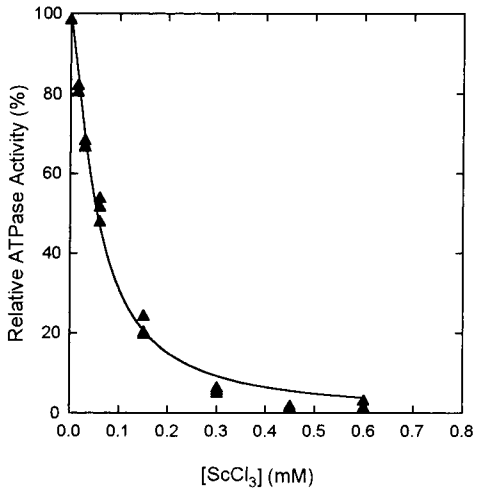

FIGURE 1: Effect of $ScCl_3$ on ATPase activity of wild-type F_1. F_1 was passed through two 1 mL centrifuge columns of Sephadex G-50 in 50 mM Tris−SO_4, pH 8.0, and preincubated at room temperature for 60 min in 50 mM Tris−SO_4, pH 8.0, containing 10 mM NaF, 2.5 mM $MgSO_4$, 1 mM NaADP, and indicated concentrations of $ScCl_3$. 100 μL aliquots (4−8 μg) were removed and assayed for ATPase activity as described in Experimental Procedures.

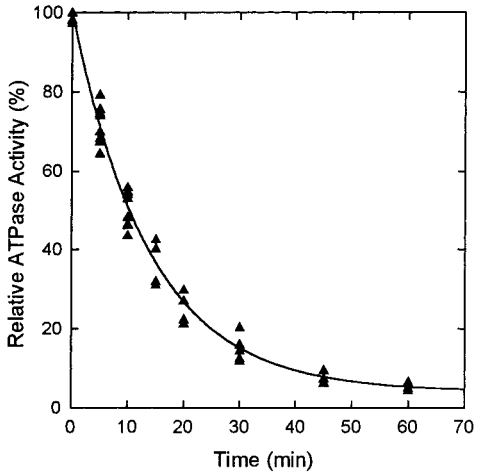

FIGURE 2: Time course of inhibition of wild-type F_1 by MgADP−fluoroscandium. F_1 was passed through two 1 mL centrifuge columns of Sephadex G-50 in 50 mM Tris−SO_4, pH 8.0, and preincubated at room temperature in 50 mM Tris−SO_4, pH 8.0, containing 0.3 mM $ScCl_3$, 10 mM NaF, 2.5 mM $MgSO_4$, and 1 mM NaADP. 100 μL aliquots (4−8 μg) were removed at indicated time intervals and assayed for ATPase activity as described in Experimental Procedures.

able to substitute for MgADP (lines 5 and 6). Omission of $MgSO_4$ resulted in prevention of the potent inhibition seen with the Mg−nucleotides (line 7). Exactly parallel results were obtained with the mutant enzymes, βY331W and βF148W, both of which have previously been shown to exhibit ATPase activities similar to that of wild-type F_1 (*28*, *38*). It should be noted that partial inhibition occurred in the presence of $MgSO_4$, $ScCl_3$, and NaF, without addition of ADP (line 8). We suspected that this inhibition could result from endogenous nucleotide being released from noncatalytic sites and then, rather than rebinding to noncatalytic sites, being instead trapped in catalytic sites by binding tightly with ScFx. A similar phenomenon was seen with AlFx (*29*). To test this possibility, we depleted the enzyme of noncatalytic-site-bound nucleotide (see footnotes *b* and *c* of Table 1). The experiments in lines 9 and 10 of Table 1 showed that removal of endogenous noncatalytic-site nucleotide did indeed reduce the inhibition significantly (residual inhibition is presumably due to small amounts of ADP still bound to the enzyme). Overall, data in this section indicated that ScFx inhibits F_1 by forming a tight-binding ternary complex with MgADP (F_1·MgADP·ScFx) at a catalytic site or sites.[3]

Dependence of inhibition of ATPase activity in wild-type F_1 on concentration of $ScCl_3$ in the presence of 2.5 mM $MgSO_4$, 1 mM ADP, and 10 mM NaF is shown in Figure 1. Half-maximal inhibition was obtained with 0.06 mM $ScCl_3$ and nearly complete inhibition with 0.5 mM $ScCl_3$. The time course of inhibition of activity, displayed in Figure 2, showed that half-maximal inhibition occurred within 10 min but full inhibition required 60 min. The rate constant for inhibition in the presence of 0.3 mM $ScCl_3$ was 1.15×10^{-3} s^{-1}, and the calculated second-order rate constant for complex formation was 3.8 M^{-1} s^{-1}. This low value suggests that inhibition does not proceed by a simple collisional process but rather that ScFx first binds to F_1·MgADP and this is followed by a slow isomerization step to yield the final F_1·MgADP·ScFx-inhibited complex. A similar conclusion was reached in relation to inhibition of myosin ATPase activity by ScFx (*33*) and has been reported in multiple papers to be the case for inhibition of myosin, P-glycoprotein, and F_1-ATPase by Vi, AlFx, or BeFx. The data of Figures 1 and 2 were obtained with wild-type enzyme; parallel results were seen with both βY331W and βY148W enzymes.

Reactivation of ATPase Activity after Inhibition by MgADP and Scandium Fluoride. Vignais and colleagues had previously shown that MgADP·BeFx irreversibly inhibits bovine mitochondrial F_1, whereas MgADP·AlFx forms an inhibitory complex which is quasi-irreversible (*23*, *24*). Here we measured reversibility of the inhibitory complexes formed between wild-type *E. coli* F_1 and MgADP·ScFx, MgADP·AlFx, and MgADP·BeFx. F_1 was preincubated with MgADP and fluorometal to produce >95% inhibition as described in the Figure 3 legend. It was then passed sequentially through two centrifuge columns to remove unbound ligands, EDTA was added, and samples were incubated at room temperature and checked for recovery of ATPase activity over a period of 100 h. EDTA was present in at least 12.5 excess over F_1 (mol/mol), and since it has very high affinity for Sc, Be, and Al ions, it served to trap all metal that was released from F_1. Figure 3 shows that F_1 preinhibited by MgADP·ScFx (triangles) slowly regained ATPase activity in a single-exponential reactivation process (solid line) with a half-time of 12 h. In contrast, F_1 inhibited by MgADP·BeFx (squares) remained inhibited over the whole 100 h time period. F_1 inhibited by MgADP·AlFx (circles) regained activity with a half-time of ~100 h (these data were not well fit by a single-exponential reactivation process; thus no line is drawn through them in the figure). Control F_1, preincubated in buffer alone, retained full activity throughout the experiment. This experiment establishes that inhibition by MgADP·

[3] $GaCl_3$ in combination with NaF was found to be a potent inhibitor of myosin ATPase, with properties similar to those of ScFx and AlFx (*35*, *47*). We found here that $GaCl_3$ in combination with NaF had no inhibitory effect on *E. coli* F_1-ATPase. Similarly, although Vi has been shown (*26*) to inhibit rat liver mitochondrial F_1-ATPase (and a wide range of other ATPases), we did not detect inhibition of *E. coli* F_1-ATPase by Vi.

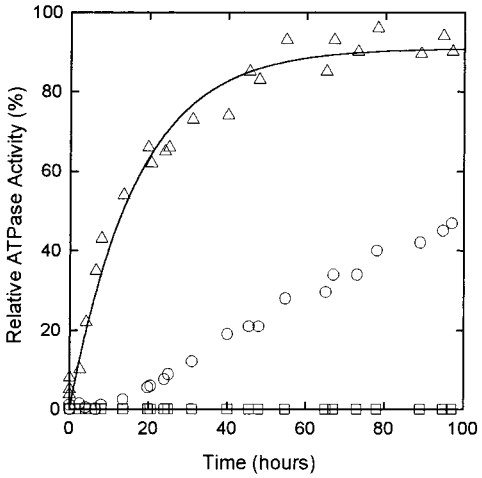

FIGURE 3: Reactivation of wild-type F_1 that had been preinhibited by MgADP−fluoroscandium, MgADP−fluoroaluminate, or MgADP−fluoroberyllate. F_1 was passed through two 1 mL centrifuge columns of Sephadex G-50 in 50 mM Tris−SO_4, pH 8.0, and then was preincubated for 60 min at room temperature in buffer containing the following additions: (Δ) 0.3 mM $ScCl_3$, 10 mM NaF, 2.5 mM $MgSO_4$, and 1 mM NaADP; (○) 0.5 mM $AlCl_3$, 10 mM NaF, 2.5 mM $MgSO_4$, and 1 mM NaADP; (□) 1.0 mM $BeSO_4$, 10 mM NaF, 2.5 mM $MgSO_4$, and 1 mM NaADP. Each sample was passed sequentially through two 1 mL centrifuge columns of Sephadex G-50 in 50 mM Tris−SO_4, pH 8.0, and EDTA was added to a final concentration of 50 or 100 μM (same results obtained). Duplicate 5 μL aliquots (4−8 μg) were removed at indicated time intervals and assayed for ATPase activity as described in Experimental Procedures. Results are from three independent experiments.

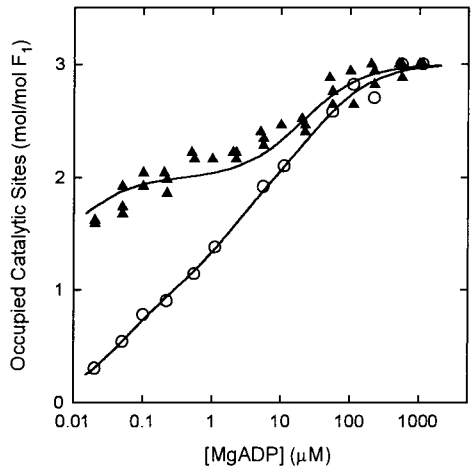

FIGURE 4: Titration of βY331W F_1 with MgADP in the presence or absence of fluoroscandium. F_1 was prepared by passage through two 1 mL centrifuge columns of Sephadex G-50 in 50 mM Tris−SO_4, pH 8.0: (○) absence of fluoroscandium; (▲) presence of fluoroscandium. The lines are fits to a model assuming three binding sites of different affinities.

ScFx is noncovalent in nature and that MgADP·ScFx is trapped tenaciously in the catalytic sites.

Titration of βY331W F_1 with MgADP in the Presence of $ScCl_3$ and NaF. The genetically engineered β-Trp-331 has a fluorescence signal which is quenched upon addition of nucleotide, enabling catalytic site nucleotide binding affinities and stoichiometries to be determined (*28*). Here we monitored binding of MgADP to βY331W F_1 in the presence and absence of $ScCl_3$ plus NaF.[4] Control experiments showed that neither NaF nor $ScCl_3$ alone had any influence on MgADP binding to βY331W F_1 (data not shown). Data for MgADP binding in the absence of ScFx (Figure 4 circles) were similar to those previously published (*28*, *41*). These data were well fit by a model assuming three binding sites of different affinities, with calculated binding parameters being $K_{d1} = 0.04$ μM, $K_{d2} = 1.8$ μM, and $K_{d3} = 34.8$ μM. The data for MgADP binding in the presence of ScFx (Figure 4, triangles) were very different. Values for these binding parameters, using a three-site model as above, were $K_{d1} < 1$ nM, $K_{d2} < 0.01$ μM, and $K_{d3} = 20.5$ μM. The K_{d1} and K_{d2} values should be considered as upper estimates only, since the first catalytic site was already filled at the lowest concentration of added MgADP. It can, however, be stated with certainty that ScFx greatly enhanced MgADP binding affinity at both catalytic sites 1 and 2, whereas it had little effect at site 3. The data confirm that ScFx inhibits F_1-ATPase by forming a tightly bound catalytic site MgADP·ScFx complex and raise the serious possibility that both catalytic sites 1 and 2, but not site 3, can form a transition state conformation.

We repeated the experiments of Figure 4 in the absence of Mg^{2+} to determine whether free ADP binding was enhanced by ScFx. The results (data not shown) were that, in the absence of Mg^{2+}, ADP bound to all three catalytic sites with equal affinity (K_{d1}, K_{d2}, $K_{d3} = 29$ μM), as expected from previous work (*40*, *41*), and that ScFx did not significantly change this pattern. Additionally, we carried out MgADP binding experiments as in Figure 4, but using βT156A/βY331W mutant F_1. Residue β-Thr-156 is a direct ligand of the Mg^{2+} in substrate MgATP or product MgADP bound at catalytic sites, and MgADP binding curves in this mutant resemble free ADP binding curves in the parent βY331W (*40*) because the Ala mutation removes the Mg^{2+}-coordinating hydroxyl oxygen. We found no enhancement of MgADP binding by ScFx in βT156A/βY331W mutant F_1. These data confirm that it is the MgADP·ScFx complex that causes inhibition and show that Mg^{2+} is required, as expected for a transition state analogue.

Effect of Fluoroscandium on MgADP Binding to βK155Q/βY331W and αR376Q/βY331W Mutant F_1. Residues β-Lys-155 and α-Arg-376 are critical for steady-state catalysis and essential for stabilizing the catalytic transition state (*31*, *32*, *48*). Panels A and B of Figure 5 show MgADP binding titrations for the mutant enzymes βK155Q/βY331W and αR376Q/βY331W, respectively. In both enzymes, MgADP binding in the presence or absence of ScFx was identical, showing that ScFx had no effect on MgADP binding affinity. These data confirm that the F_1·MgADP·ScFx complex mimics a catalytic transition state.

Fluorescence Signal of β-Trp-148 F_1 Provides a Direct Optical Probe of the Catalytic Transition State. The genetically introduced β-Trp-148 in βF148W mutant F_1[5] provides a valuable fluorescent probe of F_1 catalytic sites, because its signal shows differential responses to bound nucleoside triphosphate vs nucleoside diphosphate (*38*, *49*). Figure 6

[4] $ScCl_3$ (0.3 mM) with or without 2.5 mM $MgSO_4$ and 10 mM NaF showed no optical absorbance in the wavelength range 230−450 nm.

[5] β-Trp-148 is the only Trp residue present in βF148W mutant F_1 (*38*).

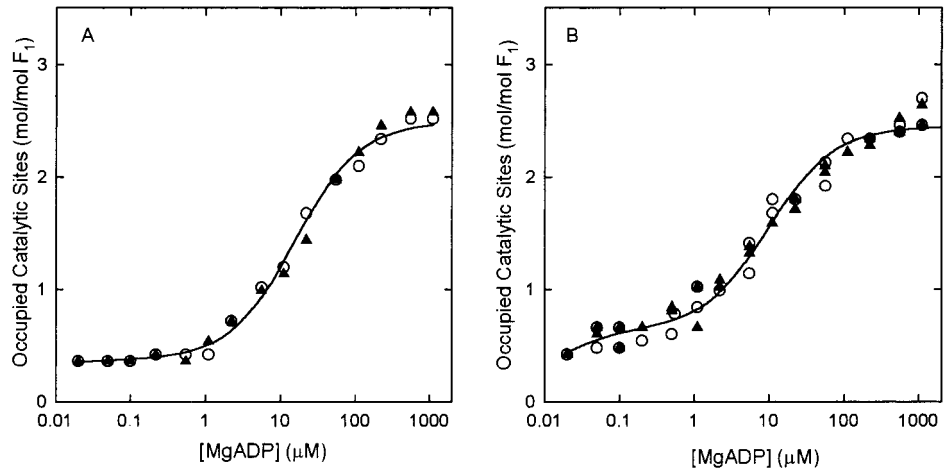

FIGURE 5: Titration of βK155Q/βY331W F_1 and αR376Q/βY331W F_1 with MgADP in the presence or absence of fluoroscandium: (A) βK155Q/βY331W F_1; (B) αR376Q/βY331W F_1; (○) absence of fluoroscandium; (▲) presence of fluoroscandium.

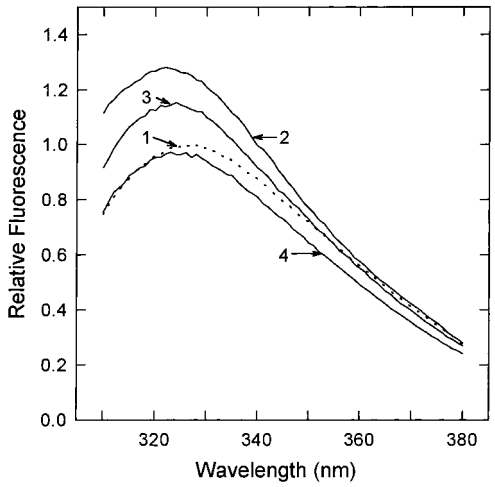

FIGURE 6: Effect of MgADP−fluoroscandium on the tryptophan fluorescence spectrum of βF148W F_1. Curves: 1 (dotted line), βF148W F_1 in buffer (50 mM Tris−SO_4, pH 8.0); 2, βF148W F_1 in buffer plus 2.5 mM $MgSO_4$, 0.3 mM $ScCl_3$, and 10 mM NaF, with 22 μM NaADP (no increase was observed at concentrations up to 1 mM NaADP); 3, βF148W F_1 in buffer plus 1 mM MgAMPPNP; 4, βF148W F_1 in buffer plus 1 mM MgADP.

shows fluorescence spectra of βF148W enzyme alone (curve 1), together with spectra obtained in the presence of MgADP·ScFx (curve 2), MgAMPPNP (curve 3), and MgADP (curve 4). It is seen that MgADP·ScFx caused a large increase of fluorescence emission, together with a blue shift. Neither effect occurred if Mg^{2+} was omitted. Relative fluorescence emission at 325 nm, with βF148W alone as baseline, was MgADP·ScFx, +28%; MgAMPPNP, +14%; and MgADP, −3%. MgADP·BeFx (an MgATP analogue) and MgATP plus azide gave the same fluorescence increase as MgAMP-PNP, and MgADP·AlFx gave the same increase as MgADP·ScFx. These data demonstrate that the β-Trp-148 fluorescence signal provides a direct optical probe of the catalytic transition state, in addition to discriminating the ATP-bound and ADP-bound ground states.

Titration of the β-Trp-148 fluorescence enhancement as a function of MgADP·ScFx concentration should in principle allow one to decide whether the whole +28% enhancement is derived just from MgADP·ScFx binding at site 1 or from binding at sites 1 and 2. This would address the important question as to whether a transition state conformation is able

Table 2: Binding of MgIDP and MgIDP·ScFx to βY331W F_1[a]

ligand	K_{d1} (μM)	K_{d2} (μM)	K_{d3} (μM)
MgIDP	1.2	100	3500
MgIDP·ScFx	<0.1	1.1	1900
MgADP	0.04	1.8	34.8
MgADP·ScFx	<0.001	<0.01	20.5

[a] Fluorescence experiments were carried out as described in Figure 4, except that MgIDP substituted for MgADP. K_d values were calculated as described in Experimental Procedures. Values for MgADP and MgADP·ScFx from Figure 4 are included for comparison.

to form only at site 1 or at both sites 1 and 2. However, MgADP·ScFx binds very tightly; for example, as Figure 4 demonstrates in βY331W F_1, 0.1 μM MgADP·ScFx was already sufficient to fill both catalytic sites 1 and 2. This poses two experimental difficulties, first that most of the MgADP added becomes bound to the enzyme and calculation of unbound MgADP is then imprecise, and second that determination of the true MgADP concentration (as opposed to ADP) is itself subject to error.

Titration of the Catalytic Sites with MgIDP·ScFx. We had shown previously that in wild-type *E. coli* F_1 K_M(MgITP) was significantly higher than K_M(MgATP) and MgIDP bound with lower affinity than MgADP (*43* and unpublished work). MgIDP·ScFx was potently inhibitory (Table 1). We carried out fluorescence titrations to determine K_d values for MgIDP and MgIDP·ScFx in βY331W F_1, and the results are shown in Table 2 (lines 1 and 2). Figure 7A (triangles) shows the titration curve for βY331W F_1 with MgIDP·ScFx. The K_d for filling of site 1 was very low, but the K_d for filling of site 2 was 1.1 μM, which is significantly higher than the corresponding value for MgADP·ScFx (Table 2, line 4) and within a range where titration can be carried out confidently.

In Figure 7B (triangles) titration of βF148W F_1 with MgIDP·ScFx is shown, and it is apparent that the same maximal enhancement of fluorescence of β-Trp-148 is achieved with MgIDP·ScFx at saturation (+27%) as with MgADP·ScFx (+28%, Figure 6). By comparison of panels A and B of Figure 7 (triangles) it is clear that maximal fluorescence enhancement is reached when site 2 has just been filled. The dotted line in Figure 7B is a fit to the MgIDP·ScFx (triangles) data, assuming that the change in fluorescence enhancement caused by filling of site 1 is equal to that caused by filling of site 2 and that filling of site 3

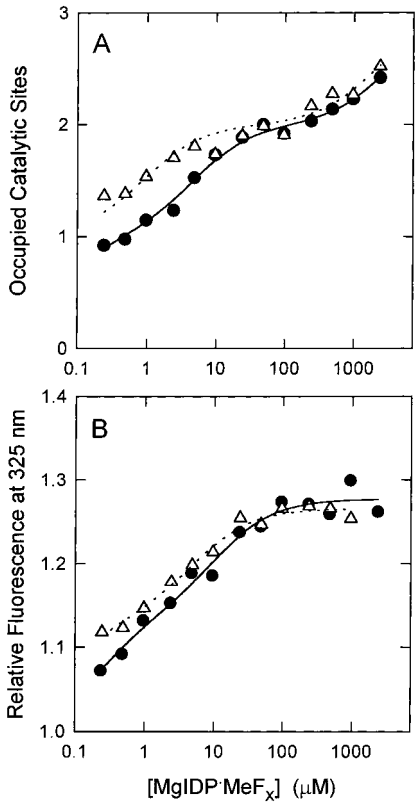

FIGURE 7: (A) Titration of βY331W F_1 with MgIDP in the presence of ScFx or AlFx: (triangles) titration with NaIDP in the presence of 2.5 mM $MgSO_4$, 0.3 mM $ScCl_3$, and 10 mM NaF; (circles) titration with NaIDP in the presence of 2.5 mM $MgSO_4$, 1.0 mM $AlCl_3$, and 10 mM NaF. The lines are fits to a model assuming three binding sites of different affinities. (B) Titration of βF148W F_1 with MgIDP in the presence of ScFx or AlFx: (triangles) titration with NaIDP in the presence of 2.5 mM $MgSO_4$, 0.3 mM $ScCl_3$, and 10 mM NaF; (circles) titration with NaIDP in the presence of 2.5 mM $MgSO_4$, 1.0 mM $AlCl_3$, and 10 mM NaF. The lines are fits to the data assuming that sites 1 and 2 contribute equal increments to the fluorescence enhancement and that site 3 contributes zero.

does not contribute to fluorescence enhancement. The data indicate that both sites 1 and 2 adopt the same transition state conformation with MgIDP·ScFx.

Panels A and B of Figure 7 (circles) show parallel experiments using MgIDP·AlFx instead of MgIDP·ScFx. Figure 7A (circles) presents titration of βY331W F_1 with MgIDP·AlFx, yielding K_d values of <0.1 μM, 5 μM, and 3.2 mM for binding to sites 1, 2, and 3, respectively. These values are significantly higher than the corresponding values for MgADP·AlFx (*29*). Figure 7B shows titration of βF148W F_1 with MgIDP·AlFx. Maximal fluorescence at saturation was +28%, the same as with MgADP·AlFx, and it is evident from comparison of panels A and B of Figure 7 (circles) that maximal fluorescence enhancement occurs when site 2 has just been filled. The solid line in Figure 7B is a fit to the MgIDP·AlFx (circles) data, assuming that equal incremental change of fluorescence enhancement occurs on filling of site 1 and site 2, with no enhancement caused by filling of site 3. These data further support the conclusion that both sites 1 and 2 form a transition state conformation.

One point that should be discussed in relation to interpretation of these experiments is that data for filling of sites are derived using βY331W F_1 (Figure 7A) whereas βF148W F_1 fluorescence is used to probe the transition state conformation (Figure 7B). The question arises as to how similar these two enzymes are in terms of nucleotide-binding parameters. Both have been well characterized (*28*, *38*). βF148W shows somewhat weaker nucleotide binding; for example, K_M(MgATP) is 45 μM for βY331W and 195 μM for βF148W (parallel value for wild type = 90 μM), and parameters for MgADP and MgAMPPNP binding differ by similar ratios. This was reflected by the data of Figure 7B, because calculation of K_d values for filling of site 2 from the fits indicated that these values were elevated 2-fold (MgIDP·AlFx) and 5-fold (MgIDP·ScFx) in βF148W as compared to βY331W. Therefore, the conclusion that both sites 1 and 2 contribute to fluorescence enhancement in βF148W F_1 is well supported.

DISCUSSION

General. This work establishes three main points: (1) MgADP−fluoroscandium (MgADP·ScFx) is a new analogue of the catalytic transition state in F_1-ATPase, (2) the fluorescence signal of β-Trp-148 in βF148W mutant enzyme is greatly enhanced by MgADP·ScFx or MgIDP·ScFx, providing the first direct optical probe of the catalytic transition state, and (3) titration of βF148W fluorescence enhancement with MgIDP·ScFx demonstrates that in F_1-ATPase both catalytic sites 1 and 2 can assume a catalytic transition state conformation simultaneously. Currently discussed models of F_1-ATPase catalytic mechanism envisage that, even under V_{max} conditions where all three sites are occupied by Mg−adenine nucleotide, only one site hydrolyzes MgATP at any one time (*51*). The new data presented here bring this assumption into question.

MgADP−Fluoroscandium Is a Catalytic Transition State Analogue. MgADP in combination with ScFx was found to form a noncovalent but very tightly bound and potently inhibitory complex at the catalytic sites of the F_1 sector of ATP synthase. MgADP·ScFx was bound at both catalytic sites 1 and 2 with greatly enhanced affinity as compared to MgADP alone, but little effect was seen at catalytic site 3. ScFx-enhanced ADP binding was Mg^{2+} dependent. Removal of β-Lys-155 and α-Arg-376 side chains, both of which are involved in forming the catalytic transition state (*31*, *32*, *48*), negated the effects of ScFx on MgADP binding. These data together demonstrate that MgADP·ScFx is acting as a transition state analogue. The Sc−O bond distance of 2.07−2.18 Å (see the introduction) is consistent with this conclusion.

β-Trp-148 Fluorescence Enhancement Provides the First Direct Optical Probe of the Catalytic Transition State. Addition of MgADP·ScFx to the βF148W enzyme caused a substantial enhancement of fluorescence, by +28% at 325 nm. In contrast, nucleoside triphosphate analogues MgAMP-PNP and MgADP·BeFx, or MgATP in the presence of azide, gave +14% enhancement, and MgADP gave −3% quench. This fluorescence enhancement provides the first direct optical probe of the transition state. MgADP·AlFx, another transition state analogue, gave the same degree of fluorescence enhancement as MgADP·ScFx. In the X-ray structure of F_1-ATPase (*50*), residue β-Phe-148 is stacked against residue β-Phe-312 in both βDP (MgADP-containing) and βTP (MgAMPPNP-containing) catalytic sites, whereas in the βE (empty) site, the two Phe residues are arranged end-on

to each other. It is likely that rearrangements of the relative positions of these two residues are responsible for the different fluorescence signals seen under different conditions of catalytic site occupancy.

The Transition State Is Mimicked at Catalytic Sites 1 and 2, but Not Site 3, by MgADP·ScFx. Recently, we reviewed models for MgATP hydrolysis by F_1-ATPase (*51*), noting that all current models make the assumption that only one catalytic site hydrolyzes MgATP at any one time, although direct evidence for this assumption is lacking. In previous work (*29*) we noted that AlFx enhanced binding affinity for MgADP at both sites 1 and 2, but not at site 3, and we discussed the implications of this finding, proposing that a true transition state complex formed at site 1 and a partial transition state-like structure formed at site 2. It is pertinent to note that previous literature had established clearly that, at saturation, the stoichiometry of MgADP·AlFx bound to F_1 was 2 mol/mol (*24*, *25*, *27*).

The new data with MgADP·ScFx reported here caused us to reconsider whether a true transition state might also form at site 2, because there was greatly enhanced binding of MgADP by ScFx at both sites 1 and 2 (Figure 4). With the β-Trp-148 fluorescence as a direct optical probe, and using the more weakly binding MgIDP·ScFx, we were able to examine this possibility experimentally. The data of Figure 7 showed that the large fluorescence enhancement of β-Trp-148 seen on addition of MgIDP·ScFx is caused in approximately equal parts by binding at sites 1 and 2. The same result was found with MgIDP·AlFx. Therefore, at least when fluorometal analogues of the transition state are used, a transition state-like conformation is able to form at both catalytic sites 1 and 2. This does not prove that, during steady-state catalysis, two sites are hydrolyzing MgATP simultaneously or that, if they are, they both contribute equally to the overall turnover rate. Sites 1 and 2 differ considerably in binding affinity for the nucleoside diphosphate−fluorometal complex; thus they are not identical in structure even with the transition state analogue bound. Nevertheless, the data certainly suggest that two sites have the potential to hydrolyze MgATP simultaneously and that the current dogma that only one site is catalytically active at any one time may be incorrect.

ACKNOWLEDGMENT

We thank Christine Schaner for excellent technical assistance.

REFERENCES

1. Henry, G. D., Maruta, S., Ikebe, M., and Sykes, B. D. (1993) *Biochemistry 32*, 10451−10456.
2. Maruta, S., Henry, G. D., Sykes, B. D., and Ikebe, M. (1993) *J. Biol. Chem. 268*, 7093−7100.
3. Fisher, A. J., Smith, C. A., Thoden, J. B., Smith, R., Sutoh, K., Holden, H. M., and Rayment, I. (1995) *Biochemistry 34*, 8960−8972.
4. Schlichting, I., and Reinstein, J. (1997) *Biochemistry 36*, 9290−9296.
5. Xu, Y. W., Morera, S., Janin, J., and Cherfils, J. (1997) *Proc. Natl. Acad. Sci. U.S.A. 94*, 3579−3583.
6. Smith, C. A., and Rayment, I. (1996) *Biochemistry 35*, 5404−5417.
7. Sondek, J., Lambright, D. G., Noel, J. P., Hamm, H. E., and Sigler, P. B. (1994) *Nature 372*, 276−279.
8. Coleman, D. E., Berghuis, A. M., Lee, E., Linder, M. E., Gilman, A. G., and Sprang, S. R. (1994) *Science 265*, 1405−1412.
9. Scheffzek, K., Ahmadian, M. R., Kabsch, W., Wiesmuller, L., Lautwein, A., Schmitz, F., and Wittinghofer, A. (1997) *Science 277*, 333−338.
10. Rittinger, K., Walker, P. A., Eccleston, J. F., Smerdon, S. J., and Gamblin, S. J. (1997) *Nature 389*, 758−762.
11. Schindelin, H., Kisker, C., Schlessman, J. L., Howard, J. B., and Rees, D. C. (1997) *Nature 387*, 370−376.
12. Tesmer, J. J. G., Berman, D. M., Gilman, A. G., and Sprang, S. R. (1997) *Cell 89*, 251−261.
13. Rayment, I. (1996) *J. Biol. Chem. 271*, 15850−15853.
14. Rees, D. C., and Howard, J. B. (1999) *J. Mol. Biol. 293*, 343−350.
15. Weber, J., and Senior, A. E. (1997) *Biochim. Biophys. Acta 1319*, 19−58.
16. Nakamoto, R. K., Ketchum, C. J., and Al-Shawi, M. K. (1999) *Annu. Rev. Biophys. Biomol. Struct. 28*, 205−234.
17. Noji, H., Yasuda, R., Yoshida, M., and Kinosita, K. (1997) *Nature 386*, 299−302.
18. Kato-Yamada, Y., Noji, H., Yasuda, R., Kinosita, K., and Yoshida, M. (1998) *J. Biol. Chem. 273*, 19375−19377.
19. Sambongi, Y., Iko, Y., Tanabe, M., Omote, H., Iwamoto-Kihara, A., Ueda, I., Yanagida, T., Wada, Y., and Futai, M. (1999) *Science 286*, 1722−1724.
20. Dimroth, P., Kaim, G., and Matthey, U. (2000) *J. Exp. Biol. 203*, 51−59.
21. Fillingame, R. H., Jiang, W., and Dmitriev, O. Y. (2000) *J. Exp. Biol.*, 9−17.
22. Rastogi, V. K., and Girvin, M. E. (2000) *Nature 402*, 263−268.
23. Lunardi, J., Dupuis, A., Garin, J., Issartel, J. P., Michel, L., Chabre, M., and Vignais, P. V. (1988) *Proc. Natl. Acad. Sci. U.S.A. 85*, 8958−8962.
24. Issartel, J. P., Dupuis, A., Lunardi, J., and Vignais, P. V. (1991) *Biochemistry 30*, 4726−4733.
25. Dupuis, A., Issartel, J. P., and Vignais, P. V. (1989) *FEBS Lett. 255*, 47−52.
26. Ko, Y. H., Bianchet, M., Amzel, L. M., and Pedersen, P. L. (1997) *J. Biol. Chem. 272*, 18875−18881.
27. Dou, C., Grodsky, N. B., Matsui, T., Yoshida, M., and Allison, W. S. (1997) *Biochemistry 36*, 3719−3727.
28. Weber, J., Wilke-Mounts, S., Lee, R. S. F., Grell, E., and Senior, A. E. (1993) *J. Biol. Chem. 268*, 20126−20133.
29. Nadanaciva, S., Weber, J., and Senior, A. E. (1999) *J. Biol. Chem. 274*, 7052−7058.
30. Nadanaciva, S., Weber, J., and Senior, A. E. (1999) *Biochemistry 38*, 7670−7677.
31. Nadanaciva, S., Weber, J., Wilke-Mounts, S., and Senior, A. E. (1999) *Biochemistry 38*, 15493−15499.
32. Braig, K., Menz, R. I., Montgomery, M. G., Leslie, A. G. W., and Walker J. E. (2000) *Structure 8*, 567−573.
33. Gopal, D., and Burke, M. (1995) *J. Biol. Chem. 270*, 19282−19286.
34. Maruta, S., Homma, K., and Ohki, T. (1998) *J. Biochem. 124*, 578−584.
35. Park, S., Ajtai, K., and Burghardt, T. P. (1997) *Biochemistry 36*, 3368−3372.
36. Anderson, T. J., Neuman, M. A., and Melson, G. A. (1973) *Inorg. Chem. 12*, 927−930.
37. Atwood, J. L., and Smith, K. D. (1974) *J. Chem. Soc., Dalton Trans.*, 921−923.
38. Weber, J., Bowman, C., and Senior, A. E. (1996) *J. Biol. Chem. 271*, 18711−18718.
39. Rao, R., Al-Shawi, M. K., and Senior, A. E. (1988) *J. Biol. Chem. 263*, 5569−5573.
40. Weber, J., Hammond, S. T., Wilke-Mounts, S., and Senior, A. E. (1998) *Biochemistry 37*, 608−614.
41. Löbau, S., Weber, J., Wilke-Mounts, S., and Senior, A. E. (1997) *J. Biol. Chem. 272*, 3648−3656.
42. Weber, J., and Senior, A. E. (2000) *Biochemistry 39*, 5287−5294.

43. Weber, J., Lee, R. S. F., Grell, E., Wise, J. G., and Senior, A. E. (1992) *J. Biol. Chem. 267*, 1712−1718.
44. Weber, J., Wilke-Mounts, S., and Senior, A. E. (1994) *J. Biol. Chem. 269*, 20462−20467.
45. Senior, A. E., Lee, R. S-F., Al-Shawi, M. K., and Weber, J. (1992) *Arch. Biochem. Biophys. 297*, 340−344.
46. Taussky, H. H., and Shorr, E. (1953) *J. Biol. Chem. 202*, 675−685.
47. Maruta, S., Uyehara, Y., Homma, K., Sugimoto, Y., and Wakabayashi, K. (1999) *J. Biochem. 125*, 177−185.
48. Senior, A. E., Nadanaciva, S., and Weber, J. (2000) *J. Exp. Biol. 203*, 35−40.
49. Weber, J., and Senior, A. E. (1998) *J. Biol. Chem. 273*, 33210−33215.
50. Abrahams, J. P., Leslie, A. G. W., Lutter, R., and Walker, J. E. (1994) *Nature 370*, 621−628.
51. Weber, J., and Senior, A. E. (2000) *Biochim. Biophys. Acta 1458*, 300−309.

BI000941O